Journal of
Materials Chemistry C

Materials for optical, magnetic and electronic devices

Accepted Manuscript

This article can be cited before page numbers have been issued, to do this please use: K. Jejen, S. Derenko, A. Cortés-Villena, J. Abad, J. F. González-Martínez, R. E. Galian, M. Sessolo and F. Palazon, *J. Mater. Chem. C*, 2025, DOI: 10.1039/D5TC00346F.

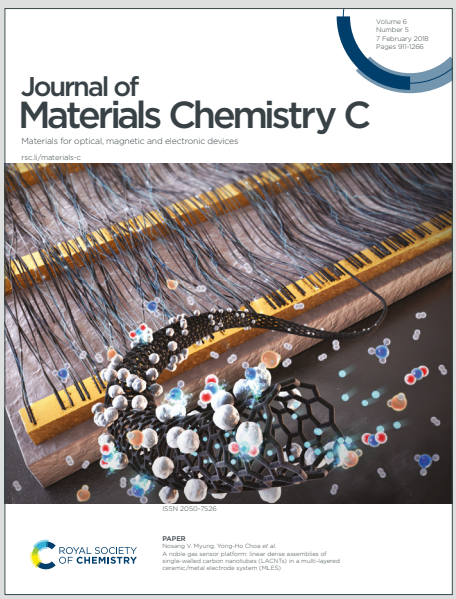

ROYAL SOCIETY OF CHEMISTRY

rsc.li/materials-c

View Article Online
DOI: 10.1039/D5TC00346F

ARTICLE

Spray-coated $CsPbBr_3$/$CsPb_2Br_5$ thin film photodetectors from nanocrystalline inks

Received 00th January 20xx,
Accepted 00th January 20xx

DOI: 10.1039/x0xx00000x

Katherine Jejen,[a] Serhii Derenko,[b] Alejandro Cortés-Villena, [b] José Abad,[c] Juan F. González-Martínez,[c] Raquel E. Galián,[b] Michele Sessolo,[b] and Francisco Palazon*[a]

Herein, we developed a simple approach for the fabrication of thin film inorganic perovskite and perovskite-related photoconductors. First, we synthesized $CsPbBr_3$ and $CsPb_2Br_5$ nanoinks solutions under near-ambient conditions. Second, we demonstrated the deposition of thin films with tunable properties from these nanoinks by a scalable spray-coting process with a commercial airbrush at low temperature. Eventually, the photoresponse of different films was recorded under monochromatic blue light. The photocurrent increases linearly with input power and achieves over three orders of magnitude differences between photocurrent and dark current.

Introduction

Halide perovskites have emerged as promising materials for optoelectronic devices due to their favorable optoelectronic properties. These materials have found applications in perovskite light-emitting diodes, photodetectors, lasers, and solar cells.[1–6] Among them, inorganic halide perovskites and related phases such as $CsPbBr_3$, $CsPb_2Br_5$, as well as dual-phase compositions, are particularly promising.[4,5,7] In 2020, Wang et al. [5] reported the photoresponse of single $CsPb_2Br_5$ nanosheets, demonstrating the potential of this material for photodetectors, despite its known wide bandgap. Previously, Tong et al.[7] fabricated dual-phase $CsPbBr_3$-$CsPb_2Br_5$ photodetectors by vacuum deposition on rigid and flexible substrates. This dual phase effectively creates a type-I heterojunction, reducing charge carrier recombination and improving the photodetectors' performances. Recently, a similar heterostructure was fabricated by Sun et al.[4] combining nanocrystal synthesis and thermal evaporation to yield composite $CsPb_2Br_5$-nanowires/$CsPbBr_3$ thin film photodetectors with high stability against humidity.

However, achieving simple, scalable fabrication methods under ambient conditions with low temperature deposition remains a challenge, as noted from the above references and others.[1,4,5,7,8]

In this work, we develop $CsPbBr_3$ and $CsPb_2Br_5$ nanocrystals inks at room temperature that are further used for the one-step deposition of thin films, using readily available commercial airbrush technology. This approach offers significant advantages in scalability compared to existing techniques. We investigated the effects of deposition temperature and the number of deposited layers on the morphological, optical, and optoelectronic response of the films. Our results reveal an optimal combination of these parameters that yields high-quality films suitable for lateral photodetectors. These films exhibit good sensitivity under blue light, demonstrating the potential of our simple synthetic approach.

Results and discussion

Nanoinks. $CsPbBr_3$ perovskite nanocrystal (NC) inks were synthesized at room temperature in nitrogen following a previously reported procedure[9] with minor adaptations (see Figure 1 and Supplementary information for more experimental details). In short, a Cs^+ precursor dissolved in propionic acid (PrAc) was injected into a mixture of hexane (HEX) and 2-propanol (iPA). Then, $PbBr_2$ precursor, dissolved in a mixture of Octanoic acid (OcAc), 2-propanol (iPA) and Octylamine (OcAm) was swiftly added. The solution turns green in just a few seconds. After redispersion in toluene, the inks can be used for further characterization and deposition of thin films.

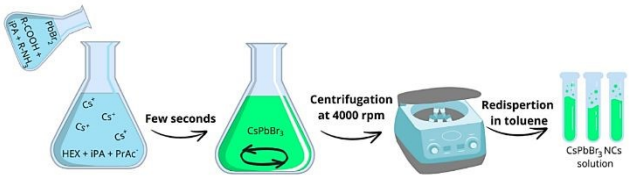

Figure 1. Schematic illustration of the synthesis, where $PbBr_2$ precursor can be dissolved with long or short chain ligands, (R could be butyl or Octyl) and the Cs precursor is in a hexane and 2-propanol mixture.

[a] Multifunctional Inorganic Materials Group, Universidad Politécnica de Cartagena, 30203 Cartagena, Spain.
[b] Instituto de Ciencia Molecular, Universidad de Valencia, 46980 Paterna Valencia, Spain.
[c] Grupo de Materiales Avanzados para la Producción y Almacenamiento de Energía, Universidad Politécnica de Cartagena, 30203 Cartagena, Spain.

View Article Online
DOI: 10.1039/D5TC00346F

Figure 2b shows the X-ray diffractogram (XRD) of $CsPbBr_3$ NCs. A perfect match with reference $CsPbBr_3$ orthorhombic phase (whose 3D crystal structure is shown in Figure 2a) is observed. Moreover, beyond 3D $CsPbBr_3$, two-dimensional $CsPb_2Br_5$ (see crystal structure in Figure 2a) has also been identified as a promising material for optoelectronics by several authors.[7,10–13] We were able to obtain this phase by adding a small amount of pure $PbBr_2$ to $CsPbBr_3$ nanoinks and letting it react for 72h at 55 °C. Transmission electron microscopy (TEM) images (Figure S1a and b) revealed that the 3D phase of $CsPbBr_3$ predominantly exhibits platelet-shaped crystals with a thickness of less than 10nm and a lateral size around 20nm. The introduction of lead bromide ($PbBr_2$) resulted in a significant morphological transformation. Specifically, the crystal structure shifted towards a majority of nano-sheets coexisting with the 3D phase and unreacted $PbBr_2$. This process also induced substantial crystal growth, yielding larger crystals with sizes between 10 and 160 nm. Consequently, the addition of $PbBr_2$ altered not only the crystallographic structure but also the overall morphology of the material. Both colloidal solutions remain however highly polydisperse in size and shape. Figure 2c shows a good match with reference $CsPb_2Br_5$ XRD pattern and a preferential orientation or growth along the c-axis, as indicated by the dominant peak at 2θ=11.7° related to the (002) plane. Nevertheless, the original 3D phase can also be observed in lower amount (Figure S1c). It is possible that core-shell structures may form, as noted by others,[26] although we do not have sufficient imaging resolution to confirm this (Figure S1b).

It is interesting to note that others have obtained $CsPb_2Br_5$ NCs directly by increasing the concentration or reaction time in a standard hot-injection colloidal $CsPbBr_3$ synthesis approach.[10] To test this in our case, we modified the synthesis by doubling the volume (at same nominal concentration of 0.5 M) of the $PbBr_2$ precursor dissolved either in a mixture of shorter chain ligands, propionic acid (PrAc) and butylamine (BuAm); (Figure 2d) or longer ligands octanoic acid (OcAc) and Octylamine (OcAm) (Figure 2e). Fig 2d exhibits a poor correlation with the diffraction patterns of either orthorhombic $CsPbBr_3$ or tetragonal $CsPb_2Br_5$. In contrast, samples synthesized using longer ligands (Fig 2e) demonstrate a significant correspondence with the orthorhombic $CsPbBr_3$ phase albeit accompanied by unidentified diffraction peaks at low-angle regions, indicating the presence of an additional, undetermined phase. These low-angle diffraction peaks in both cases are most likely ascribed to quasi-2D Ruddlesden-Popper (RP) phases with chemical formulas $BuAm_2Cs_{n-1}Pb_nBr3_{n+1}$ and $OcAm_2Cs_{n-1}Pb_nBr_{3n+1}$[14,15] Precise determination of the "n" value proves challenging due to the potential for nanostructure self-assembly. This phenomenon aligns with previous reports demonstrating that ligand substitution induces spontaneous self-assembly into larger, cuboidal $CsPbBr_3$ structures composed of multiple-stacked nanoplatelets isolated, as directly confirmed by small-angle X-ray diffraction[16] These quasi-2D crystals do not show significant changes after 30 minutes. It must be noted that, compared to the aforementioned report on direct $CsPb_2Br_5$ NC synthesis, we are using here considerably shorter alkyl ligands instead of oleylamine and oleic acid, which may explain a preferential formation of the corresponding Ruddlesden-Popper phases.

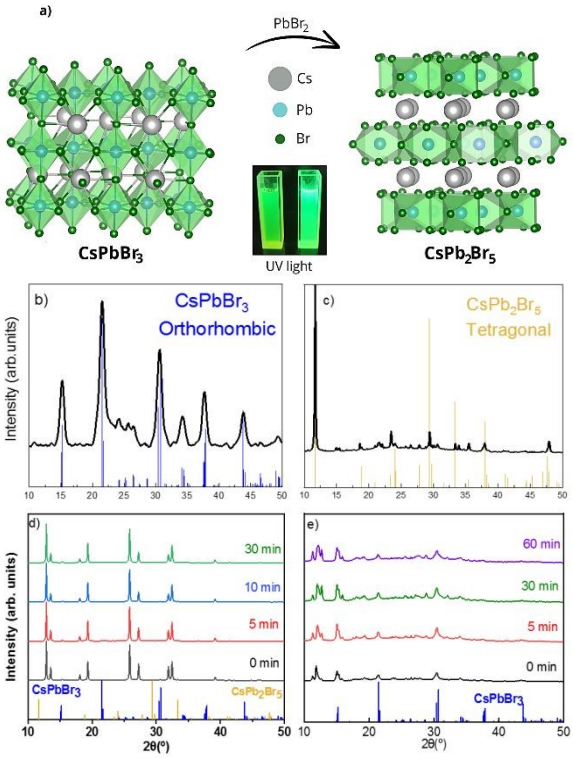

Figure 2. (a) Crystal structures of $CsPbBr_3$ orthorhombic perovskite and non-perovskite $CsPb_2Br_5$ tetragonal phase and their solutions respectively, under UV light. (b) XRD pattern of $CsPbBr_3$ orthorhombic phase (ICSD 243735) (c) XRD pattern of $CsPb_2Br_5$ tetragonal phase (ICSD 254290) Note that further details on this pattern are provided in Figure S1c(d) XRD patterns of $CsPbBr_3$ with precursor dissolved in short chain ligands (e) XRD pattern of $CsPbBr_3$ with precursor dissolved in long chain ligands. See main text for more details.

Optical characterization (Figure 3) confirm the XRD observations. The optical bandgap energy of $CsPbBr_3$ nanoink solution was determined by Tauc Plot (see Figure S1d in Supplementary information) extrapolating the straight-line portion with a bandgap energy of 2.35 eV, as expected for pure $CsPbBr_3$ nanocrystals (NCs) reported in previous works[17–20] and confirmed by the PL peak at 520 nm (Figure 3a). $CsPb_2Br_5$ nanoinks show very similar optical properties (Fig. 3b), as has already been noted by others.[1,21–24] While XRD shows a dominant $CsPb_2Br_5$ phase (Figure 2b), we already discussed above that also $CsPbBr_3$ impurities exist in the $CsPb_2Br_5$ solution which, while being small, may have an important effect especially on the photoluminescence properties. Interestingly, the PLQY of this mixed-phase solution was higher than the original 3D solution (25.6% vs 7.6%). We attribute this mainly to the surface passivating effect of adding excess $PbBr_2$ as discussed by others.[27] Figure 3c-d shows the UV-Vis and PL spectra of NCs synthesized with an excess of $PbBr_2$ precursor in BuAm or OcAm. First of all, it is important to note that the synthesis time, between 0 minutes and 30 minutes, does not affect the optical properties which is in line with the very similar XRD signals already observed previously (Figure 2d-e). Again,

View Article Online
DOI: 10.1039/D5TC00346F

these blue-shifted absorption and PL spectra are consistent with RP quasi-2D perovskites.[25] In the case of BuAm (Figure 3c) two absorption peaks are clearly present, pointing to the coexistence of different n-values for the RP phases. In the case of OcAm (Figure 3d) we observe a significant shift between the main absorption and PL peak. While the observed spectral shift could be attributed to an intrinsic Stokes shift within the RP phases, a more plausible explanation involves the presence of $CsPbBr_3$ nanocrystals (NCs) in the solution. In fact, we observe a similar photoluminescence (PL) signal also in the BuAm-based solution when it is irradiated for longer times (see Figure S2 in Supplementary information), pointing towards a possible laser-induced transformation of the RP to 3D $CsPbBr_3$.

In summary, the as-obtained hybrid organic-inorganic quasi-2D RP phases do not seem highly stable. Therefore, for the following (thin film spray-coating and optoelectronic devices), we focus solely on the inorganic $CsPbBr_3$ and $CsPb_2Br_5$ NC inks.

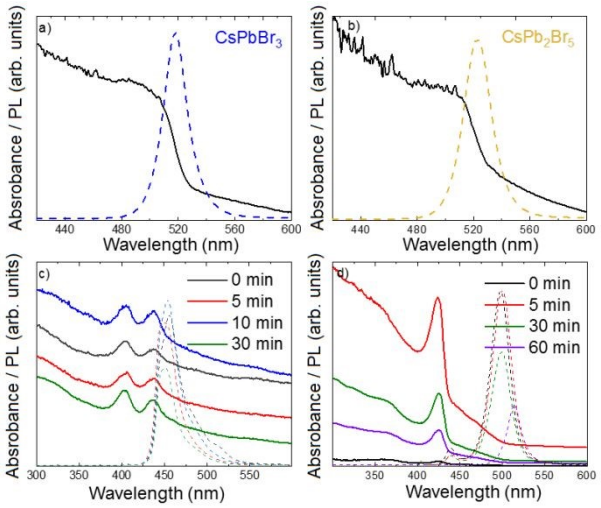

Figure 3. UV-Vis absorption and PL emission spectra of (a) $CsPbBr_3$ nanoink solution (b) $CsPb_2Br_5$ nanoink solution (c) $CsPbBr_3$ with short chain ligands (d) $CsPbBr_3$ with long chain ligands.

Spray-coated thin films. Thin films were deposited from the $CsPbBr_3$ and $CsPb_2Br_5$ nanoinks solutions on glass substrates by spray-coating using a simple commercial airbrush as shown in Figure 4. In short, the nanoinks are placed in the airbrush cup and a nitrogen gas flow with a pressure of 0.4 bar is manually controlled to blow the inks through a 0.2 mm nozzle opening onto the substrate (around 10 cm away from the nozzle) which may be heated on a hot plate to allow instant solvent evaporation. The technique is essentially additive and arbitrary volumes may be used to increase the film thickness. Here we typically used 100 µl for one layer, with the possibility of depositing multiple layers as will be discussed hereafter.

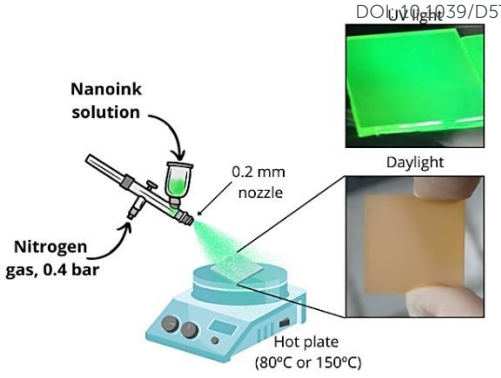

Figure 4. Schematic illustration of the spray-coating process and layers under UV light and daylight.

XRD, UV-vis absorption and photoluminescence spectra of thin films obtained with $CsPbBr_3$ and $CsPb_2Br_5$ nanoinks solutions at different temperatures and with increasing number of layers are presented in Figure 5 and 6.

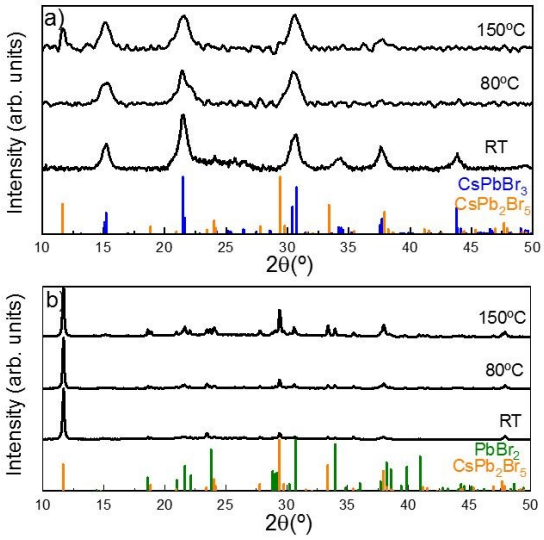

Figure 5. X-ray diffractograms of $CsPbBr_3$ and $CsPb_2Br_5$ deposited at room temperature, 80°C and 150°C (a) $CsPbBr_3$ nanoink (b) $CsPb_2Br_5$ nanoink. Reference patterns for $CsPbBr_3$ (ICSD 243735), $CsPb_2Br_5$ (ICSD 254290) and $PbBr_2$ (ICSD 239760) in blue, orange, and green respectively.

Figure 5a shows that the films deposited from $CsPbBr_3$ nanoink solution present a good match with orthorhombic crystal lattice of $CsPbBr_3$ for the samples deposited at room temperature and 80°C. The original nanocrystalline phase is thus maintained in the thin films. When the perovskite is deposited on a substrate at 150°C, a signal for tetragonal crystal lattice of $CsPb_2Br_5$ perovskite appears along with the $CsPbBr_3$ orthorhombic phase thus yielding a dual-phase $CsPb_2Br_5/CsPbBr_3$ film. Films prepared with $CsPb_2Br_5$ nanoink solution deposited at room temperature show a good match with tetragonal crystal lattice of $CsPb_2Br_5$ alongside few traces of $PbBr_2$. When increasing deposition temperature at 80°C and 150°C the peaks of $PbBr_2$ and $CsPb_2Br_5$ increase their intensity (Figure 5b) as may be

View Article Online
DOI: 10.1039/D5TC01465

expected from simple crystal sintering and growth, but no significant phase transformation is seen. Note that traces of nanocrystalline $CsPbBr_3$ may also be present but not detected by XRD.

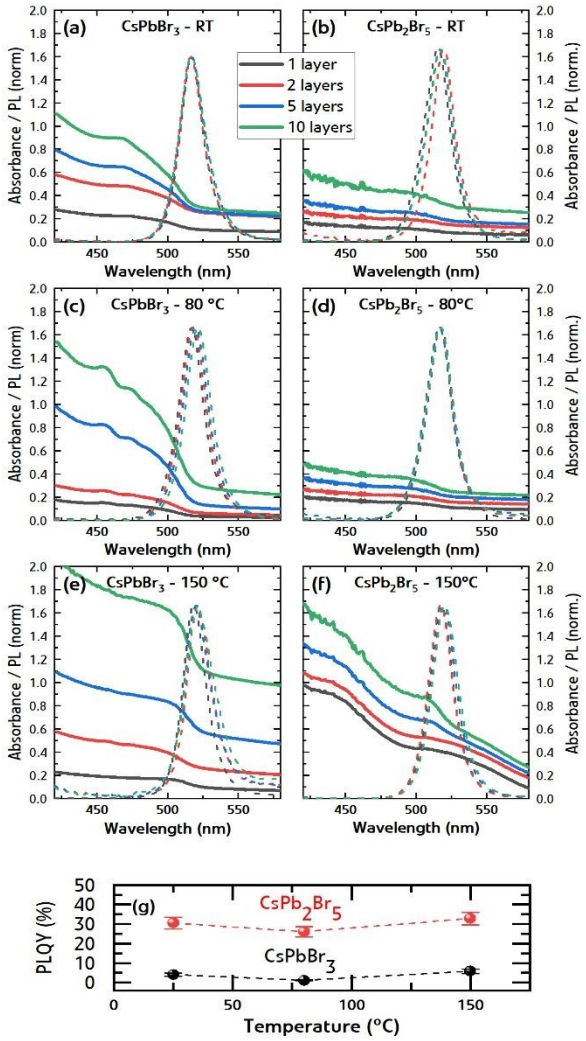

Figure 6. UV-vis absorption and PL emission spectra of $CsPbBr_3$ and $CsPb_2Br_5$ nanoinks deposited at (a-b) room temperature (c-d) 80°C (e-f) 150°C and (g) PLQY correlated with temperature deposition for $CsPbBr_3$ and $CsPb_2Br_5$

Figure 6 shows the UV-vis absorption and photoluminescence spectra (PL) of $CsPbBr_3$ and $CsPb_2Br_5$ films prepared at room temperature (Figure 6a-b), 80 °C (Figure 6c-d), and 150 °C (Figure 6e-f) respectively, with 1, 2, 5, and 10 layers (i.e., 100, 200, 500 and 1000 µL of nanoink solution). In all cases a bandgap of around 525 nm is obtained. In detail, the samples exhibited photoluminescence (PL) spectra within the range of 515 – 522 nm, corresponding to energies of 2.40 – 2.37 eV (Table S1 in supplementary information). A slight red-shift of approximately 23 meV was observed in some samples with increasing film thickness. This red-shift is consistent with previously published findings, which report red shifts in the range 0 – 30 meV attributed to enhanced self-absorption[28,29].

The increase in absorption with the number of layers translates an obvious increase in film thickness. In Figure S3, we plotted the absorbance value at 450nm for the different compositions, temperature, and number of layers. The roughly linear increase with the number of layers could serve as indication for layer thickness. Nonetheless, we note that absorbance values are derived from transmission measurements neglecting scattering (reflectance) which may be significant for some samples. Photoluminescence quantum yield (PLQY) (Figure 6g) was measured for $CsPbBr_3$ and $CsPb_2Br_5$ films prepared with 5 layers (500 µL of nanoink solution) deposited at room temperature, 80°C and 150°C. The lower absorption but higher PLQY of the $CsPb_2Br_5$ films suggests, as previously hypothesized, that these films embed small but brightly emissive $CsPbBr_3$ clusters, passivated by a $PbBr_2$-rich shell.

Thickness of $CsPbBr_3$ and $CsPb_2Br_5$ thin films deposited at 80°C and 150°C were characterized by atomic force microscopy (see Supplementary Information Figure S4 and S5) (samples prepared at room temperature were disregarded as poor homogeneity was found already by eye). While accurate thickness determination may be difficult due to the high roughness of the films, an obvious increase from around 10nm to few hundreds of nanometers is observed when increasing the number of layers from 1 to 10 (see Table S2). The morphology of $CsPbBr_3$ and $CsPb_2Br_5$ layers was further analysed employing scanning electron microscopy (SEM; Figure 7 and S6). Films deposited from $CsPbBr_3$ inks show better homogeneity, with less aggregates than films deposited from $CsPb_2Br_5$ (Figure 7). For the thicker films (10 layers), it is possible to see some cracks (Figure S6) but, as the films are grown by successive layer deposition, it is not obvious to determine whether the cracks penetrate the whole film thickness.

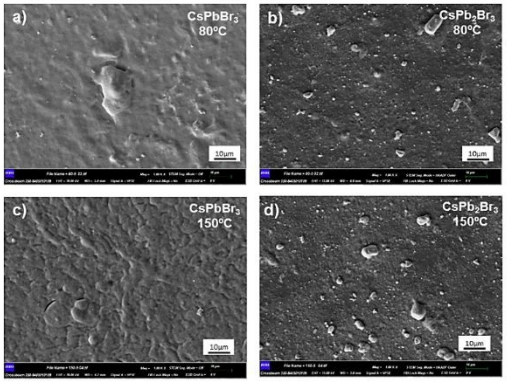

Figure 7. Scanning electron microscopy (SEM) surface images of 5 layers of $CsPbBr_3$ and $CsPb_2Br_5$ deposited (a-b) at 80°C, (c-d) at 150°C.

The films were also characterized by X-ray photoelectron spectroscopy (XPS) to verify the oxidation state of Cs, Pb and Br (Figure S7) and the stoichiometry. The +1 oxidation state of Cs was verified in all cases by the peaks at 724.0 and 738.0 eV corresponding to the Cs 3d5/2 and Cs 3d3/2 orbitals. Similarly, Br 3d5/2 and Br 3d3/2 peaks at 68.0 and 69.5 eV correspond to the expected bromide signals for $CsPbBr_3$ and $CsPb_2Br_5$. Eventually, the main Pb 4f signals at 138.0 and 143.0 eV are consistent with Pb(II), with a minor contribution at lower

View Article Online DOI: 10.1039/D5TC00746B

binding energy ascribed to Pb(0). This metallic lead has been extensively observed before in lead halide perovskites and may be induced by ionizing radiation such as employed in XPS. [30] The stoichiometry derived from XPS for films deposited at 80 °C and 150 °C from both inks is summarized in Table 1.

Table 1. XPS quantification of thin films deposited from $CsPbBr_3$ and $CsPb_2Br_5$ nanoinks at different temperatures. Expected values for pure-phase $CsPbBr_3$ and $CsPb_2Br_5$ are given in red.

Nanoink	Deposition temperature	Cs at.%	Pb at.%	Br at.%
$CsPbBr_3$	80 °C	18.34 (20)	22.00 (20)	59.67 (60)
$CsPbBr_3$	150 °C	17.81 (20)	22.67 (20)	59.52 (60)
$CsPb_2Br_5$	80 °C	15.96 (12.5)	24.39 (25)	59.65 (62.5)
$CsPb_2Br_5$	150 °C	15.05 (12.5)	23.17 (25)	61.78 (62.5)

Overall, the obtained stoichiometries are close to the expected values (in red in Table 1) for $CsPbBr_3$ and $CsPb_2Br_5$. We observe however a slight Pb-rich (Cs-poor) composition for films prepared from $CsPbBr_3$ which may be related to a preferential $PbBr_2$ film termination, considering that XPS is a surface-sensitive technique. The opposite could be said about films deposited from $CsPb_2Br_5$, where a Cs-rich composition is observed. Nonetheless, as already noted in the discussion of Figure 5, it is known that the films are not phase-pure, so that the slight differences between expected and obtained stoichiometries may be simply due to the coexistence of different phases.

Lateral photodetectors. We implemented the spray-coated thin films into lateral photodetectors. For this purpose, we deposited nanoinks solutions onto interdigitated ITO substrates, each one having four identical "pixels" with 40 µm spacing between the electrodes (see Figure S8 in supporting information for a schematic representation and device details) and measured current-voltage (I-V) characteristics under different lighting conditions. As a preliminary study, we evaluated separately the effect of layer thickness at fixed deposition temperature (fig S9a) and deposition temperature at fixed film thickness (fig S9b) under dark conditions and white light (1 sun). Based on this we chose 5 layers and a deposition temperature of 150 °C as optimal conditions to maximize photocurrent, maintaining a similarly low dark current for all films. Then, I-V curves were measured under 405-nm illumination at different intensities. Figure 8 a-b present representative current-voltage measurements (Figure S10 shows good homogeneity among different pixels). Note that the dark I-V characteristics are very similar for the two compounds, due to the very high dark resistivity of this type of materials. However, the photocurrent of devices based on $CsPbBr_3$ was found to increase up to almost three orders of magnitude compared to the dark current, when increasing the light intensity up to 200 mW/cm^2. On the other hand, the $CsPb_2Br_5$ samples showed a much reduced response, with a maximum variation of the photocurrent within one order of magnitude. The lower photoconductivity might originate from the reduced connectivity of the lead halide within the layered $CsPb_2Br_5$ crystal structure. It could be expected that the preferential orientation of the $CsPb_2Br_5$ on the substrate could favor lateral transport, but as the typical crystal size is small with regards to the electrode spacing this is probably not significant (as opposed to having a single nanosheet bridging two electrodes which is not the case here). Interestingly, both materials show a linear increase in photocurrent as a function of input light power (Figure 8c). A higher slope of the current-intensity curve (sensitivity) is observed for the $CsPbBr_3$ devices, although some saturation of the photocurrent might be seen at high illumination intensity. Additionally, photocurrent was measured within the voltage range of -50V to 50V, with a reverse sweep to assess the hysteresis caused by charge accumulation at the non-ohmic ITO/semiconductor interfaces, and by ionic migration (see Figure S11 a-b in Supplementary Information). Under both dark and light conditions, both $CsPbBr_3$ and $CsPb_2Br_5$ samples demonstrated consistent I-V curves, with negligible hysteresis (the curves are in logarithmic scale). This speaks for a rather low concentration of ionic species in the material. The dynamic response of both photodetectors was also evaluated as a function of light intensity (see Figure S11 c-d). However, it must be noted that low response times as well as other relatively poor photodetector metrics such as responsivity or linear dynamic range which can partly be derived from Figure 8 may be intrinsic to the device geometry, which is a lateral photoconductor and therefore not directly comparable with vertical photodiodes. Furthermore, on/off ratios as well as responsivity and EQE vs wavelength have been evaluated showing superior performances from the CsPbBr3 devices (Figure S12) as well as in terms of rise and fall times (Figures S13). Regarding stability, it is interesting to note that after 9 months of storage in a nitrogen-filled glovebox, the devices remain essentially unchanged (see Figure S14 in Supplementary Information).

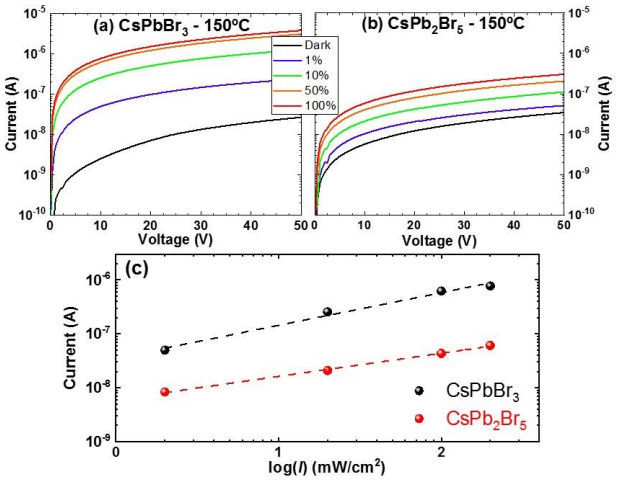

Figure 8. Current-voltage curves of (a) $CsPbBr_3$ and (b) $CsPb_2Br_5$ at 150 ºC under various illumination power using a blue light LED as source light (100% power intensity equals to 200 mW/cm²). (c) Current – intensity dependence of $CsPbBr_3$ and $CsPb_2Br_5$ at 150 ºC at 10V plotted based on previous measurements and fitted with linear function.

Conclusions

In conclusion, we have demonstrated a simple approach for the deposition of inorganic $CsPbBr_3$, $CsPb_2Br_5$ and dual-phase $CsPbBr_3$-$CsPb_2Br_5$ thin films combining low-temperature colloidal synthesis and post-synthesis modifications together with spray-coating using commercially available airbrush technology. As a result, high-quality perovskite and perovskite-related thin films are obtained with significant light absorption and emission in the visible range. Eventually, lateral photodetectors have been fabricated and dual-phase films have shown the best performances, with an increase of up to 3 orders of magnitude in photocurrent with respect to dark current under monochromatic blue light. These results are promising for the development of inexpensive perovskite optoelectronics, providing a simple and upscalable route towards device fabrication. Next studies will focus on controlling the film morphology (possibly by optimizing the viscosity and wetting properties of the solvent and surface) in order to improve charge transport, and to apply these materials to more complex functional devices such as solar cells and LEDs.

Author contributions

The manuscript was written through contributions of all authors.

Conflicts of interest

There are no conflicts to declare.

Acknowledgements

The authors acknowledge funding for project TED2021-129609BI00 funded by MCIN/AEI /10.13039/501100011033 and by the European Union NextGenerationEU/ PRTR, grant CNS2023-144331, funded by MCIU/AEI/10.13039/501100011033 and by European Union «Next Generation EU»/PRTR and Grant PID2022-139191OB-C32 funded by MCIN/AEI. F. P. acknowledges funding for grant RYC2020-028803-I funded by MCIN/AEI/10.13039/501100011033 and "ESF Investing in your future". The authors acknowledge also funding from the Generalitat Valenciana, project CISEJI/2022/43.

Notes and references

1 X. Zhang, B. Xu, J. Zhang, Y. Gao, Y. Zheng, K. Wang and X. W. Sun, *Advanced Functional Materials*, 2016, **26**, 4595–4600.
2 B.-S. Zhu, H.-Z. Li, J. Ge, H.-D. Li, Y.-C. Yin, K.-H. Wang, C. Chen, J.-S. Yao, Q. Zhang and H.-B. Yao, *Nanoscale*, 2018, **10**, 19262–19271.
3 C. Zhang, Z. Wang, M. Wang, J. Shi, J. Wang, Z. Da, Y. Zhou, Y. Xu, N. V. Gaponenko and A. S. Bhatti, *ACS Appl. Mater. Interfaces*, 2023, **15**, 35216–35226.
4 Z. Sun, Y. Wang, Y. Liu, R. Liu, T. Chen, S. Ye, N. Lai, H. Cui, F. Lin, R. Wang, J. Yang, S. Ke and C. Wang, *ACS Appl. Nano Mater.*, 2024, **7**, 11785–11793.
5 R. Wang, Z. Li, S. Li, P. Wang, J. Xiu, G. Wei, H. Liu, N. Jiang, Y. Liu and M. Zhong, *ACS Appl. Mater. Interfaces*, 2020, **12**, 41919–41931.
6 X. Zhang, Z. Jin, J. Zhang, D. Bai, H. Bian, K. Wang, J. Sun, Q. Wang and S. F. Liu, *ACS Appl. Mater. Interfaces*, 2018, **10**, 7145–7154.
7 G. Tong, H. Li, D. Li, Z. Zhu, E. Xu, G. Li, L. Yu, J. Xu and Y. Jiang, *Small*, 2018, **14**, 1702523.
8 M. Yang, J. Yu, S. Jiang, C. Zhang, Q. Sun, M. Wang, H. Zhou, C. Li, B. Man and F. Lei, *Opt. Express, OE*, 2018, **26**, 20649–20660.
9 Q. A. Akkerman, M. Gandini, F. Di Stasio, P. Rastogi, F. Palazon, G. Bertoni, J. M. Ball, M. Prato, A. Petrozza and L. Manna, *Nat Energy*, 2016, **2**, 1–7.
10 P. Acharyya, P. Pal, P. K. Samanta, A. Sarkar, S. K. Pati and K. Biswas, *Nanoscale*, 2019, **11**, 4001–4007.
11 J. Deng, J. Xun, W. Shen, M. Li and R. He, *ACS Appl. Nano Mater.*, 2021, **4**, 9213–9222.
12 Z. Zhang, Y. Zhu, W. Wang, W. Zheng, R. Lin and F. Huang, *Journal of Materials Chemistry C*, 2018, **6**, 446–451.
13 Z.-P. Huang, B. Ma, H. Wang, N. Li, R.-T. Liu, Z.-Q. Zhang, X.-D. Zhang, J.-H. Zhao, P.-Z. Zheng, Q. Wang and H.-L. Zhang, *J. Phys. Chem. Lett.*, 2020, **11**, 6007–6015.
14 M. Rahil, R. M. Ansari, C. Prakash, S. S. Islam, A. Dixit and S. Ahmad, *Sci Rep*, 2022, **12**, 2176.
15 G. Liu, C. Qiu, B. Tian, X. Pan, D. Ding, Y. Chen, C. Ren, T. He, Y. Shi, C. Su, Y. Li, Y. Gao and D. Fan, *ACS Appl. Electron. Mater.*, 2019, **1**, 2253–2259.
16 Spontaneous Self-Assembly of Cesium Lead Halide Perovskite Nanoplatelets into Cuboid Crystals with High Intensity Blue Emission, https://advanced.onlinelibrary.wiley.com/doi/epdf/10.1002/advs.201900462, (accessed March 13, 2025).
17 D. A. Idosa, M. Abebe, D. Mani, A. Thankappan, S. Thomas, F. G. Aga and J. Y. Kim, *Photonics*, 2023, **10**, 802.
18 W. Yan, L. Mao, P. Zhao, A. Mertens, S. Dottermusch, H. Hu, Z. Jin and B. S. Richards, *Opt. Express, OE*, 2020, **28**, 15706–15717.
19 K. Sung Hun, K.-D. Park and H. S. Lee, *Energies*, 2021, **14**, 275.

View Article Online
DOI: 10.1039/D5TC00346F

20 L. Protesescu, S. Yakunin, M. I. Bodnarchuk, F. Krieg, R. Caputo, C. H. Hendon, R. X. Yang, A. Walsh and M. V. Kovalenko, *Nano Lett.*, 2015, **15**, 3692–3696.
21 Q. Han, S. Gong, H. Yu and W. Wu, *Optical Materials*, 2023, **137**, 113477.
22 K. Du, L. He, S. Song, J. Feng, Y. Li, M. Zhang, H. Li, C. Li and H. Zhang, *Advanced Functional Materials*, 2021, **31**, 2103275.
23 J. Lv, L. Fang and J. Shen, *Materials Letters*, 2018, **211**, 199–202.
24 P. Li, C. Hu, L. Zhou, J. Jiang, Y. Cheng, M. He, X. Liang and W. Xiang, *Materials Letters*, 2017, **209**, 483–485.
25 S. Bhaumik, S. A. Veldhuis, Y. F. Ng, M. Li, S. K. Muduli, T. C. Sum, B. Damodaran, S. Mhaisalkar and N. Mathews, *Chem. Commun.*, 2016, **52**, 7118–7121.
26 One-Pot Synthesis of Stable CsPbBr3@CsPb2Br5 Core–Shell Heteronanocrystals with Controlled Permeability to Halide Ions | Chemistry of Materials, https://pubs.acs.org/doi/10.1021/acs.chemmater.3c01280, (accessed March 13, 2025).
27 M. I. Bodnarchuk, S. C. Boehme, S. ten Brinck, C. Bernasconi, Y. Shynkarenko, F. Krieg, R. Widmer, B. Aeschlimann, D. Günther, M. V. Kovalenko and I. Infante, *ACS Energy Lett.*, 2019, **4**, 63–74.
28 D. Baranov, S. Toso, M. Imran and L. Manna, *J. Phys. Chem. Lett.*, 2019, **10**, 655–660.
29 J. S. van der Burgt, J. J. Geuchies, B. van der Meer, H. Vanrompay, D. Zanaga, Y. Zhang, W. Albrecht, A. V. Petukhov, L. Filion, S. Bals, I. Swart and D. Vanmaekelbergh, *J. Phys. Chem. C*, 2018, **122**, 15706–15712.
30 Z. Dang, J. Shamsi, F. Palazon, M. Imran, Q. A. Akkerman, S. Park, G. Bertoni, M. Prato, R. Brescia and L. Manna, *ACS Nano*, 2017, **11**, 2124–2132.
31 Deconvoluting the energy transport mechanisms in all-inorganic CsPb2Br5/CsPbBr3 perovskite composite systems | APL Materials | AIP Publishing, https://pubs.aip.org/aip/apm/article/10/3/031101/2834855, (accessed March 28, 2025).
32 R. Zhi, J. Hu, S. Yang, C. Perumal Veeramalai, Z. Zhang, M. I. Saleem, M. Sulaman, Y. Tang and B. Zou, *Journal of Alloys and Compounds*, 2020, **824**, 153970.

View Article Online
DOI: 10.1039/D5TC00346F

In accordance with the FAIR principles, the data sustaining the manuscript *"Spray-coated CsPbBr3/CsPb2Br5 thin film photodetectors from nanocrystalline inks"*, is located (open access) at the host's academic repository:

https://repositorio.upct.es/entities/person/7ba1ef8c-072d-4f1e-9eaf-4ce322a54e4f?tab=isAuthorOfPublication.